Title

Ultrafast carrier dynamics in high-density photo-doped MoS2: monolayer vs multilayer

Journal

Journal of Physics Condensed Matter, 38(27)

ISSN

0953-8984

Authors

Khatua, Durga Prasad
Singh, Asha
Gurung, Sabina
et al.

Publication Date

2026-07-10

DOI

10.1088/1361-648x/ae82a8

Journal of Physics:
Condensed Matter

PAPER • **OPEN ACCESS**

Ultrafast carrier dynamics in high-density photo-doped MoS_2: monolayer vs multilayer

To cite this article: Durga Prasad Khatua *et al* 2026 *J. Phys.: Condens. Matter* **38** 275401

Journal of Physics: Condensed Matter

OPEN ACCESS

RECEIVED
18 March 2026

REVISED
18 June 2026

ACCEPTED FOR PUBLICATION
25 June 2026

PUBLISHED
7 July 2026

PAPER

Ultrafast carrier dynamics in high-density photo-doped MoS_2: monolayer vs multilayer

Durga Prasad Khatua[1,*], **Asha Singh**[2], **Sabina Gurung**[3] and **J Jayabalan**[4,*]

[1] Mechanical and Aerospace Engineering Department, University of California Los Angeles, Los Angeles, CA 90095, United States of America
[2] Nano Science Laboratory, Materials Science section, Raja Ramanna Centre for Advanced Technology, Indore 452013, India
[3] Department of Chemistry and York Biomedical Research Institute, University of York, York, YO10 5DD, United Kingdom
[4] Faculty for physics and CENIDE, University of Duisburg-Essen, Duisburg 47057, Germany
[*] Authors to whom any correspondence should be addressed.

E-mail: dkhatua@physics.ucla.edu and quantumbalan@gmail.com

Keywords: high-density photoexcitation, intervalley scattering, ultrafast carrier dynamics, MoS_2, undefined

Supplementary material for this article is available online

Abstract

Monolayer (MoL) and multilayer (MuL) MoS_2 are extremely fascinating materials for optoelectronics, particularly in scenarios involving high excitation carrier densities. Consequently, it is essential to understand the various processes and their associated time scales in MoL and MuL two-dimensional materials under such high excitation densities. Here, we demonstrate that carrier dynamics in MoL and MuL MoS_2 exhibit distinctly different behaviors above the Mott density, with MoL showing faster carrier relaxation and enhanced many-body interactions compared to MuL. Despite the similarity in band structure near the *K*-point and the formation of A-excitons, pronounced differences in the transient response are observed, highlighting the influence of the overall band structure. Exciton dissociation, band gap renormalization, and intervalley relaxation play a consequential role in dictating the ultrafast transient properties of these samples. The study in this paper provides a detailed understanding of the fundamental optoelectronic properties of the two-dimensional MoS_2 at high excitation densities, paving the way for its potential applications in various photonic and optoelectronic domains.

1. Introduction

Due to the increasing demand for scalable optoelectronic applications, the exploration of novel materials has led to the emergence of transition-metal dichalcogenides, a class of two-dimensional layered materials. Among them, molybdenum disulfide (MoS_2) is a highly studied material because of its tunable optoelectronic properties, which can be controlled by varying the number of layers. In particular, MoS_2 shows a transition from indirect to direct band gap as it is thinned from bulk to single-layer form [1, 2]. Due to the direct band gap nature, the monolayer (MoL) MoS_2, possesses several physical properties that make it suitable for a wide range of applications, including optoelectronics, valleytronics, and quantum technologies [3–5]. On the other hand, bulk and multilayer (MuL) MoS_2 find their applications in transistors, photodetectors, solar cells, flexible electronics, and gas and biosensors, among others [6–10].

Regardless of the number of layers, MoS_2 exhibits three types of excitons in the visible region: A, B, and C [1, 2]. In addition, owing to the significant contribution of the *d*-orbital electrons from Mo-atoms, MoS_2 exhibits high spin–orbit coupling at the *K*-point of the Brillouin zone, which is strong enough to lift the degeneracy in both the valence and conduction bands [11]. In the MoL form, quantum confinement and enhanced Coulomb interactions between charge carriers become significant, resulting in tightly bound excitons with binding energies of approximately ∼0.5 eV [12–14]. By comparison, the exciton binding energy in bulk MoS_2 is much lower, around 45 meV [15, 16], which is still larger than that of typical bulk semiconductors such as Si, Ge, InAs, and GaAs. Moreover, MoL MoS_2 exhibits

two nonequivalent yet degenerate valleys at the *K*-points as a consequence of broken inversion symmetry. In contrast, bulk MoS_2 possesses inversion symmetry, rendering the bands near the *K*-points equivalent, while the spin and optical transition properties remain similar to those of the MoL [1, 2, 15].

The application of MuL and MoL MoS_2 in optoelectronic and sensor devices necessitates a comprehensive understanding of their fundamental carrier dynamics. Investigating carrier relaxation dynamics offers valuable insight into the transient optical and electronic properties of these materials. Several research groups have studied the carrier dynamics in MoS_2 earlier to understand the carrier behavior with different excitation and probing conditions [17–27]. Until now, research has primarily focused on the carrier dynamics at low excitation densities, where perturbations in the properties due to high excitation conditions are kept to a minimum. However, several MoS_2-based applications demand handling of high excitation densities, such as optical parametric amplifier [28], modulator [29], and photodetectors [30]. Consequently, it is essential to understand the carrier dynamics at such high photo-excitation conditions.

In this work, we present the results of the carrier dynamics studied in MoL and MuL MoS_2 flakes under varying nominal photoexcited carrier densities per layer (NPL), ranging from 0.66×10^{14} cm^{-2} to 4.16×10^{14} cm^{-2} at A-exciton energy, which is above the Mott density of a MoL MoS_2 [31]. Atomic force microscope (AFM) measurements were performed to determine the number of layers in the selected MoS_2 flakes. The thickness of the MuL on which the carrier dynamics measurements were reported is 8.9 nm, which corresponds to about 11 layers of MoS_2. As previously reported, an increase in the number of layers leads to a gradual change in the optical property of the MoS_2 [1, 2, 32]. However, the properties remain almost unchanged if the number of layers goes beyond six [1, 2, 32]. Thus, the present sample with 11 layers can be treated as a bulk MoS_2. By investigating the transient carrier behavior in both of these samples, we present a comparison of the carrier relaxation pathways and their associated time constants. We find that the Auger and defect-assisted Auger processes play a crucial role in determining carrier relaxation in MoL, whereas an additional mechanism, intravalley scattering, dominates in MuL. In MoL, intervalley scattering is not prominent, as carriers are excited at the lowest transition energy, which corresponds to the A-exciton. Furthermore, the peak heights of the transient signal show a distinct saturation behavior in MuL while it remains linear in MoL MoS_2. The primary objective of the present study is to directly compare the two limiting dimensional regimes, MoL and MuL, in order to clearly elucidate the influence of reduced dimensionality on carrier dynamics at photoexcitation densities above the Mott density.

2. Result and discussion

The samples that are used in the ultrafast carrier dynamic measurements are procured from 2DLayers, USA, and are grown on sapphire substrate in the chemical vapor deposition method [33]. Figure 1(a) shows the large area absorption spectrum of the flakes, which has two distinct peaks in the lower energy region corresponding to A and B-excitons [2, 18, 34]. These peaks can be well fitted with Lorentzian functions, centered at 1.83–1.98 eV with spectral widths of 0.11–0.18 eV, respectively. In addition, the absorption spectrum of the MoL sample used for the transient studies (figure S3) shows the A- and B-exciton peaks at 1.83 eV and 1.98 eV, respectively. Microscopic optical images of the sample reveal the presence of both well-separated and partially connected MoS_2 flakes. The observed transmission contrast indicates that, although the sample consists of flakes with different thicknesses, each individual flake exhibits a constant height. Subsequent AFM measurements confirm that most flakes are MoLs, along with a few MuL flakes. The images of the specific MuL and MoL MoS_2 flakes used for the pump–probe measurements are shown in figures 1(b) and (c), respectively [35, 36]. These optical images were acquired using a home-built microscope integrated into the pump–probe setup, enabling both the identification and investigation of the selected flakes. The dotted circles in the images indicate the specific locations where transient measurements were performed in transmission mode. The thickness of the flakes was determined by performing AFM topography scans at the edges of these flakes. AFM topography scans of the MoL and MuL flakes on which the transient measurement results presented in this work are shown in figures 2(a) and (c), respectively. Furthermore, the corresponding height profiles across the edges of the MoL and MuL flakes are shown in figures 2(b) and (d), respectively. From the height differences at the edge of the flakes, the thicknesses of the MoL and MuL flakes are estimated to be nearly 0.8 nm and 8.9 nm, respectively. Further, the Raman spectrum (figure S2) confirms the single layer MoS_2. Based on the thickness of a single layer, the MuL flake is expected to be composed of 11 mono layers [1, 2, 37]. The in-plane dimensions of the MuL and MoL flakes are $\sim$35 μm and $\sim$100 μm, respectively.

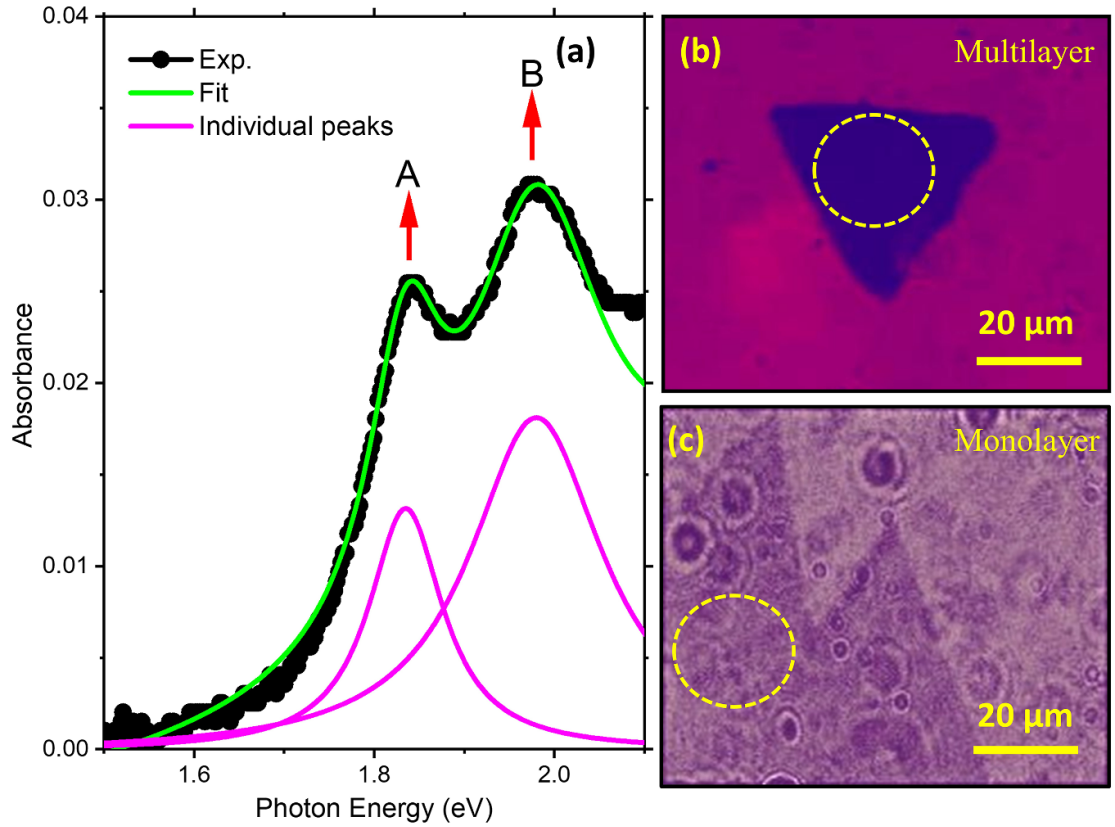

Figure 1. Optical characterization of the MuL and MoL MoS_2 flakes. (*a*) Large area averaged absorbance spectrum of the MoS_2 flakes. The solid green line represents the best fit to the data using two Lorentzian peaks shown as solid magenta lines. Optical image of the MuL MoS_2 flake (*b*), and MoL MoS_2 flake (*c*), acquired using a microscope. Dotted circles indicated the region where carrier dynamics measurements were performed. Optical image of the MoL MoS_2 in panel (c) is adapted from our previous work, [37]. Copyright © IOP Publishing. Adapted with permission under the IOP Authors Rights Policy.

All transient data presented herein were acquired using a home-built, degenerate pump–probe configuration tuned to the A-exciton transition energy (figure S1). A more detailed description of the experimental setup is provided in the supporting information (SI). In this article, all the measurements are performed in the pump fluence range, 1.2 mJ cm^{-2} to 7.5 mJ cm^{-2} which corresponds to an NPL of 6.6×10^{13} cm^{-2} to 4.1×10^{14} cm^{-2} at the A-exciton wavelength [35–37]. The NPL is calculated using a standard conversion relation, $N \propto \frac{E}{E_{ph}} \frac{A}{\pi r_{FWHM}^2}$ with N as number of photons, E as the laser pump pulse energy, A as absorbance, E_{ph} as energy of a single photon at the pump wavelength, and r_{FWHM} as the beam radius at full width half maximum on the sample, measured using a CCD camera. In this calculation, the absorption across the MuL is considered uniform across the film to first order, as the optical decay over such thickness is weak due to the higher optical penetration depth of ∼81.3 nm as calculated from the absorption coeffiecient [38]. Since measurements were carried out at such high excitation densities, it is essential to ensure that there are no permanent modifications or damage to the flakes. Pan *et al* studied structural modifications in MuL MoS_2 and found that the samples remained intact up to a pump fluence of 150 mJ cm^{-2} [23]. When they increased the fluence up to 400 mJ cm^{-2}, nanoridges and nanocracks were formed in the flakes. We have performed AFM measurements before and after our pump–probe measurements, revealing no structural changes in either MoL or MuL flakes. This indicates that the maximum fluence used in the pump–probe measurement (10 mJ cm^{-2}) is small enough to damage the flakes. Further, we have also checked that the MoL is stable even up to 50 mJ cm^{-2} [36, 37].

The fluence-dependent transient transmission signal ($\Delta T/T$) of the MuL MoS_2 flake is shown in figure 3(a). At low pump fluences, the transmission of the sample reduces with the arrival of the pump pulse and attains a negative peak near the end of the pump pulse. This change in the transmission then starts recovering as the time delay between the pump and probe increases and returns to its original unperturbed transmission state by about 5 ps. As the pump fluence increases, the magnitude of

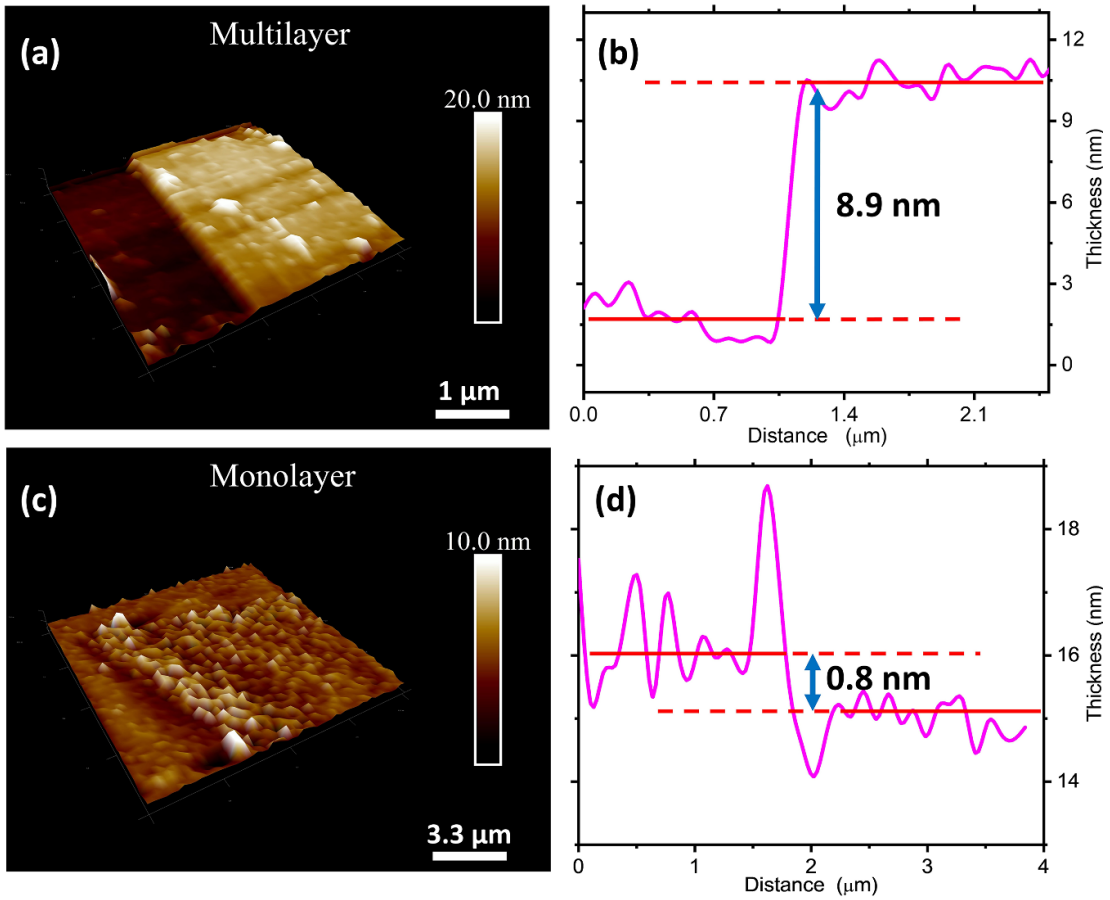

Figure 2. Panels (*a*) and (*b*): AFM topographic scan and the corresponding height profile extracted along a line perpendicular to an edge of the MuL flake, respectively. Panels (*c*) and (*d*): are the same but for the MoL flake. Panel (*d*) is adapted from our previous work, [37]. Copyright © IOP Publishing. Adapted with permission under the IOP Authors Rights Policy.

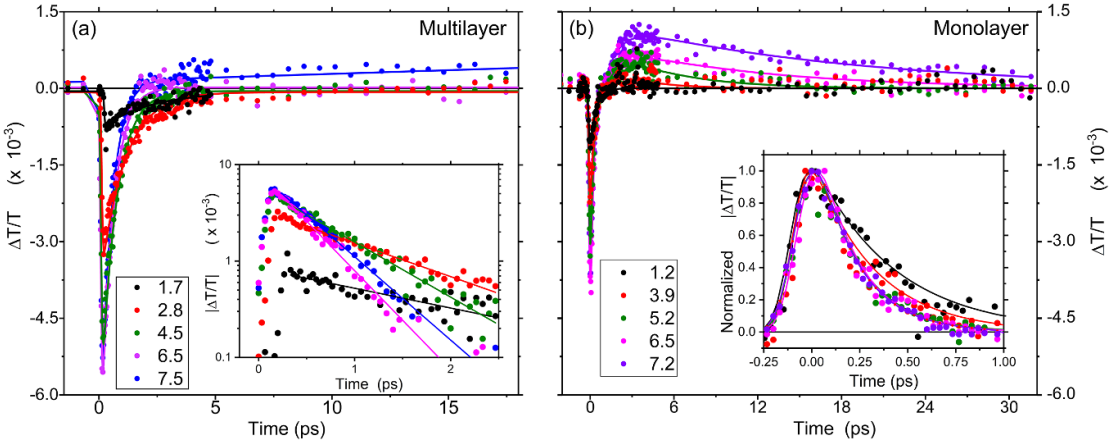

Figure 3. Fluence-dependent transient transmission signals recorded at a pump–probe wavelength of 672 nm: (a) for MuL MoS_2 flake (inset: same data on a shorter time scale is shown with a logarithmic *y*-axis), and (b) for MoL MoS_2 flake (inset: same data normalized and zoomed around zero delay time). The legend indicates the pump fluence in mJcm^{-2}.

the peak change in the transmission also increases. At higher fluence, the recovery of transmission was found to be faster than that at lower pump fluences. Furthermore, when pump fluence is <6.5 mJ cm^{-2}, the transient signal recovers completely by about 5 ps. However, as the fluence increases beyond 6.5 mJ cm^{-2}, $\Delta T/T$ was found to change its sign from negative to positive after nearly 4 ps. The inset of figure 3(a) shows the same transient signal of the MuL MoS_2 flake over the first few picoseconds, and the *y*-axis is plotted on a logarithmic scale. The solid lines in the inset plot are the linear fit to the logarithm of $|\Delta T/T|$ in 0.3 ps to 2.5 ps range. The linear relationship between the $\log(|\Delta T/T|)$ and decay

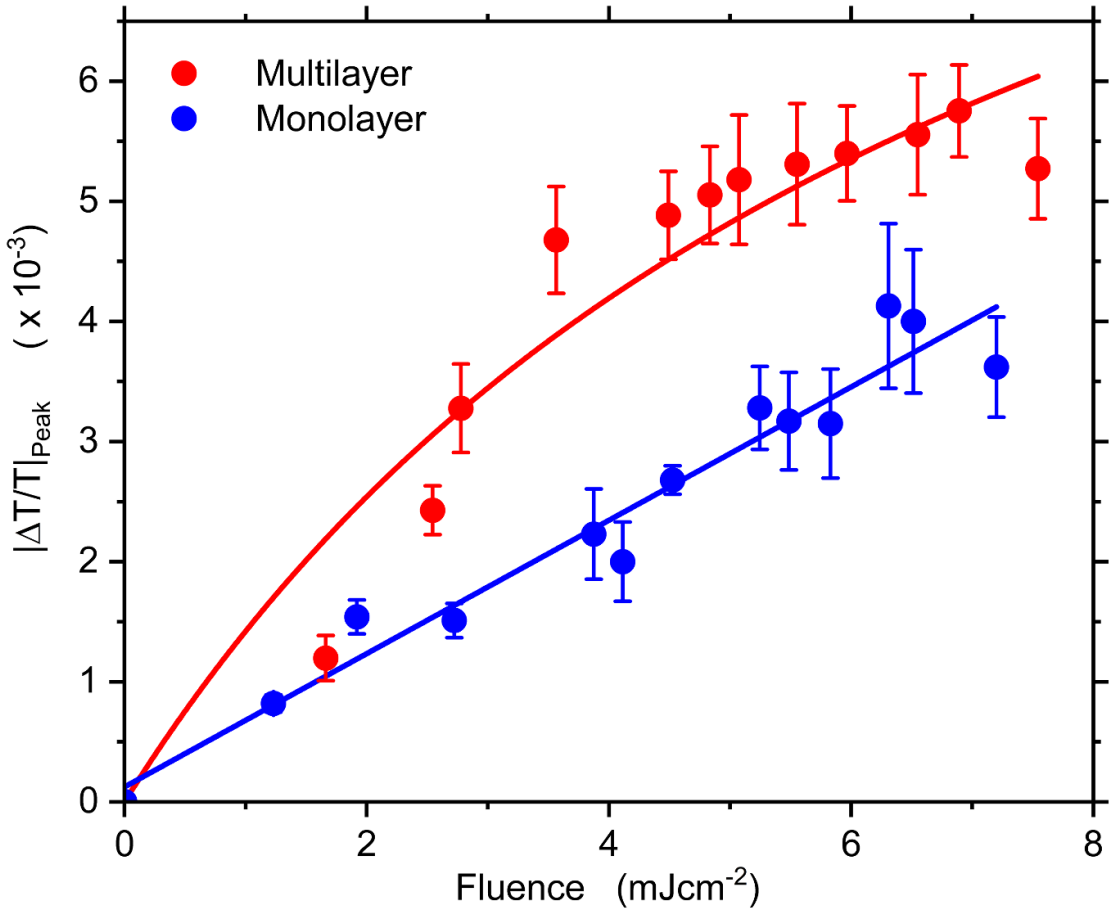

Figure 4. fluence dependence of the initial negative peak magnitude of $\Delta T/T$ for the MuL MoS_2 (red dots) and MoL MoS_2 (blue dots). The solid lines represent the best fit to the corresponding data sets.

time with a negative slope indicates that the $\Delta T/T$ shows a single exponential decay. From the slope of this linear fit, the decay time of $\Delta T/T$ can be obtained.

In figure 3(b), the transient transmission signal of the MoL MoS_2 flake is shown for the same pump fluence range as that used for the MuL flake. Similar to the MuL sample, the $\Delta T/T$ signal of the MoL MoS_2 also starts decreasing with the arrival of the pump pulse reaching a negative peak. This negative change starts recovering with increasing delay time. As the pump fluence is increased, the magnitude of the maximum change in $\Delta T/T$ also increases. At lower pump fluences, the transient signal recovers completely within the first 2 ps. However, at higher pump fluences, $\Delta T/T$ changes sign from negative to positive. This positive signal builds up slowly and attains a positive maximum by about 3 ps. In the inset of figure 3(b), the normalized $|\Delta T/T|$ of MoL MoS_2 flake is shown up to one picosecond delay between pump and probe. Clearly, the decay time of $|\Delta T/T|$ decreases with the increase in pump fluence. In addition, to assess any possible laser-induced heating effects, we measured the transient response over longer pump–probe delay times for both MoL and MuL samples, and also performed the same measurements on the sapphire substrate to evaluate its contribution to the transient signal (figure S4). No evidence of laser heating or substrate-induced effects was observed (see SI for a more detailed discussion).

Let us now compare the behavior of the MuL flake with that of MoL flake. Figure 4 shows the variation of the magnitude of the initial negative peak height of $\Delta T/T$ ($|\Delta T/T|_{Peak}$) with pump fluence for the MuL MoS_2 (red dots) and MoL MoS_2 (blue dots) samples. In the case of MuL MoS_2, the $|\Delta T/T|_{Peak}$ increases with pump fluence, but at higher fluence, the peak shows signature of saturation.

At higher excitation intensities it is possible to saturate the electronic or excitonic transitions by filling a substantial fraction of the higher energy state and also by the depletion of the initial state. This leads to a reduction in the absorption under higher excitation conditions. In this regime, the intensity-dependent absorption coefficient can be expressed as,

$$\alpha = \frac{\alpha_0}{1 + I/I_S}, \tag{1}$$

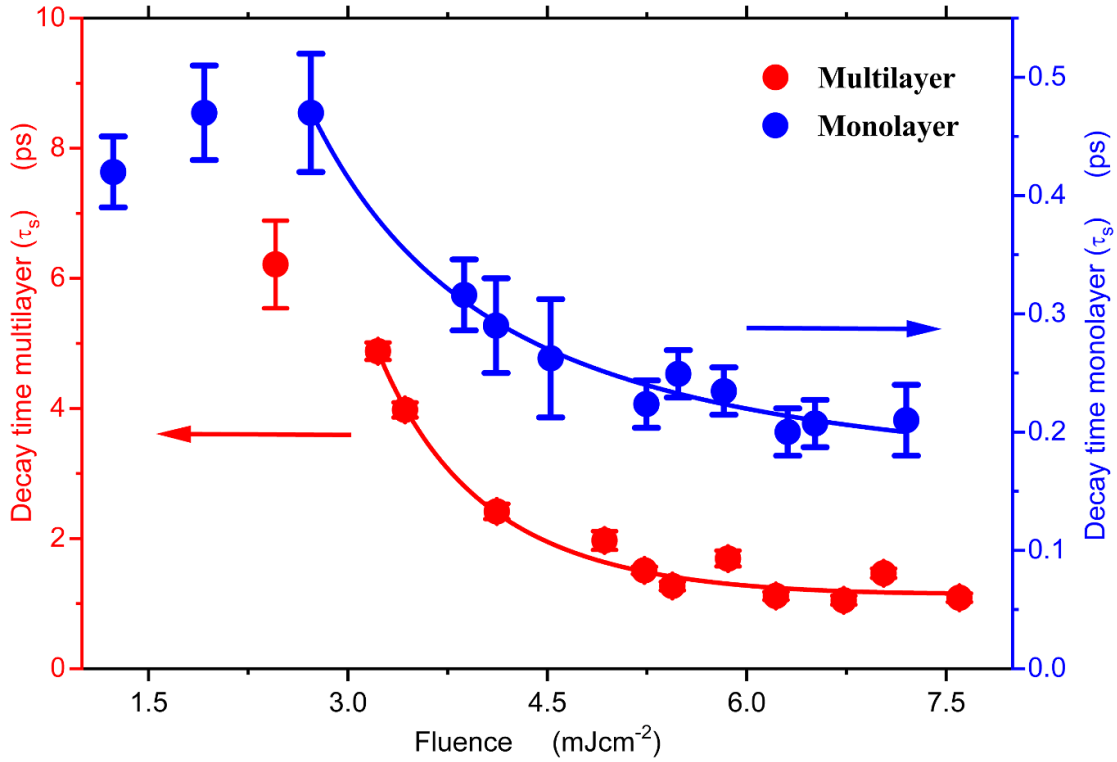

Figure 5. Pump fluence dependence of the relaxation times of the MuL (τ_{MuL}, red dots) and MoL (τ^s_{MoL}, blue dots) MoS_2 flakes. The solid lines indicate the best fits to the data.

where I and I_S are the intensity of excitation and saturation intensity of the material. In the experiment, both the temporal pulse width and spot size of the pump pulse are kept constant; therefore, the fluence (F) is directly proportional to the peak intensity of the pulse. The peak transient transmission is related to the change in absorption in the presence of pump by $\Delta T/T = -\Delta\alpha d$. Here, d is the thickness of the sample and $\Delta\alpha$ represents the pump-induced change in the absorption. Substituting α from equation (1), the peak change in the transient transmission can be expressed as,

$$\left|\frac{\Delta T}{T}\right|_{\text{Peak}} = \frac{(\alpha_0 d)F}{F+F_S}, \tag{2}$$

where F denotes the fluence used in the experiment, and F_S is the saturation fluence. The above equation was used to fit the experimentally measured data for the MuL sample and is represented as a solid red curve in figure 4. In contrast, the variation of the initial peak height $|\Delta T/T|_{\text{Peak}}$ for the MoL sample shows a linear dependence on the pump fluence (figure 4). The solid blue line shows the linear fit to the $|\Delta T/T|_{\text{Peak}}$ data for MoL MoS_2.

Having discussed about the initial negative peak change in the $\Delta T/T$, let us now compare the associated recovery time, or equivalently the decay time of $|\Delta T/T|$, τ_s, occurring at the initial short time scale. For the MuL case, the decay time τ_s at each fluence is extracted by fitting the transient data in the range of 0.3 ps to 2.5 ps to a single exponential function. The obtained best-fit decay time for various fluences is plotted in figure 5. The fluence dependence of τ_s is well described by the empirical relation $\tau = A/F^2 + B$, where, A and B are fitting constants. The corresponding best fit is also shown in figure 5. The observed decrease in relation time τ_{MuL} with $1/F^2$ suggests the involvement of nonlinear relaxation processes such as Auger recombination, carrier–carrier scattering, or exciton–exciton annihilation. In this case, the presence of higher number of excited carriers enhances the relaxation dynamics via collective effect as the threshold is being crossed.

When compared to the MuL flake, the transient transmission of MoL flakes shows more complex dynamical behavior. Following the recovery of the initial negative peak, the $\Delta T/T$ becomes positive, which subsequently recovers over much longer time scales at later times (figure 3(b)). Hence, extracting the correct recovery time in MoL is more complicated compared to MuL. A detailed discussion on the fluence dependence of the MoL flake can be found in our earlier publication [35]. However, for the sake of completeness, in short, we discuss the time dependence of the MoL sample here. To obtain the

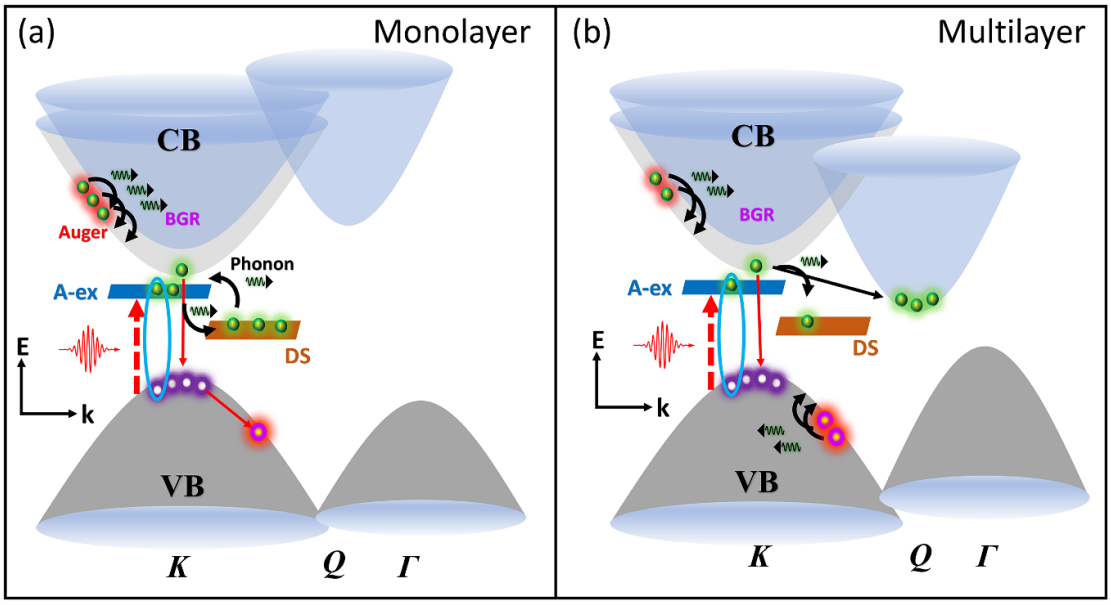

Figure 6. Simplified schematic of the band structure near the band edge and various processes that happen at femtosecond to few tens of picosecond time scale when pump photon energy is tuned to A-exciton: (*a*) MuL MoS_2 with exciton dissociation, Auger scattering, and intervalley scattering and (*b*) MoL MoS_2 exciton dissociation and Auger scattering.

fast recovery time of the MoL case, τ_s, we fit the experimental data to an empirical function,

$$\mathcal{F} = A_0\left[1+\mathcal{E}\left(\frac{t}{t_0}\right)\right]\exp\left(-\frac{t}{\tau_s}\right) + B_0\left[1-\exp\left(\frac{t-t_d}{\tau_r}\right)\right]\exp\left(-\frac{t-t_d}{\tau_L}\right). \quad (3)$$

The first part of the equation represents the initial fast negative change in the transmission and a corresponding exponential recovery with a recovery time τ_s. Here, A_0 denotes the amplitude of the initial negative transient signal, while t_0 represents its build-up time. The second term accounts for the positive $\Delta T/T$ component that emerges after the recovery of the initial negative signal. Here, τ_r describes the build-up time of this delayed positive response. The decay constant τ_L represents the subsequent relaxation of this positive component. The short-range decay time component, τ_s, for MoL MoS_2 is also plotted in figure 5. At lower pump fluences (<2.7 mJ cm^{-2}), τ_s remains almost constant around 0.4 ps. However, as the pump fluence exceeds 2.7 mJ cm^{-2}, the relaxation time decreases rapidly, showing a similar trend as that of the MuL case.

Following the recovery of negative change in transmission, the MoL flake shows a positive transmission change even at a pump fluence of 3.9 mJ cm^{-2} which subsequently increases with higher pump fluences. However, the MuL flake shows only a small positive change at the highest fluence used in the present measurements (7.5 mJ cm^{-2}). Furthermore, the positive peak in $\Delta T/T$ for the MoL sample appears around 3 ps followed by a gradual decay. In contrast, for the MuL sample, the positive change in $\Delta T/T$ remains almost constant without any noticeable recovery over tens of picoseconds of delay time.

It is well established that the electronic band structure of MoS_2 is highly dependent on the number of layers in the material [1, 2]. Figure 6, panels (a) and (b), represents a simplified schematic of the relevant band structure for MoL and MuL MoS_2. In MoL MoS_2, the material exhibits a direct bandgap at the *K* valley, where both the conduction band minimum and the valence band maximum are located [1, 2]. When two layers are stacked, a conduction band minimum emerges at the *Q* point situated in between the Γ and *K* valleys, resulting in an indirect bandgap [1]. This transition significantly reduces the photoluminescence efficiency of bilayer MoS_2 by approximately a factor of ∼40 compared to MoL MoS_2 [1]. As the number of layers increases, the conduction band minima at the *Q* point continues to decrease in energy [1, 32]. Beyond 5 to 6 layers, the changes in the band structure stabilize and become largely independent of the number of layers. Thus, the MuL flake investigated in this study is an indirect bandgap semiconductor. Despite these structural changes, the excitonic resonance energy of MuL MoS_2 remains nearly identical to that in MoL MoS_2, at 1.83 eV [1, 15]. However, the A-exciton binding energy

differs significantly in both cases: ∼45 meV in MuL which is an order of magnitude lower than in MoL MoS_2 [15, 16].

Let us now examine the dynamical processes that drive the transient optical response of the MuL compared to the MoL MoS_2 following excitation by a short laser pulse. Several groups have studied carrier dynamics in MuL and MoL MoS_2 flakes at the A-exciton transition energy and reported various physical phenomena that dominate for a few hundred of picoseconds after an ultrafast pulse excitation. The observed physical phenomena are strongly dependent on the excitation photon energy, excitation density, and probing photon energy, as well as the type of samples and delay time, making understanding of the carrier dynamics quite complicated. Various processes like exciton formation [21, 39, 40], exciton dissociation [35, 37, 41, 42], exciton–exciton annihilation [17, 18, 20, 43, 44], carrier capture to defect and trap states [45–47], Auger and defect-assisted Auger scattering [32, 34, 48, 49], hot-phonon reabsorption [22, 50], and intervalley scattering [51, 52] are likely to occur in both MuL and MoL MoS_2 flakes. These processes will lead to band bleaching [53], band gap renormalization (BGR) [50, 54], exciton peak shift and broadening [22, 43, 55], etc.

In MoL and MuL MoS_2, the exciton Mott transition typically occurs at a critical photoinduced carrier density per layer on the order of 10^{12} cm^{-2}; specifically, Liu *et al* estimated a threshold density of $\sim 4.3 \times 10^{12}$ cm^{-2} for the onset of this transition [31]. Above this critical density, enhanced Coulomb screening by the photogenerated electron–hole gas diminishes the exciton binding energy and induces exciton ionization into a correlated electron–hole plasma. This many-body regime is characterized by a severe suppression and broadening of excitonic resonances, bleaching of the A and B excitons, and pronounced BGR. In ultrafast transient absorption spectroscopy, this high-density response manifests as a characteristic combination of exciton bleaching and derivative-like or red-shifted photoinduced absorption features. This spectral profile reflects the competing dynamics between quasi-particle bandgap shrinkage and the reduction of exciton binding energy. This interpretation is strongly supported by time-resolved angle-resolved photoemission spectroscopy on MoS_2, which demonstrated a BGR of up to $\sim$ 360 meV above the Mott threshold [31]. Consequently, because the estimated NPL in this work exceeds the 10^{13} cm^{-2} regime, accompanied by pronounced exciton bleaching, our observations are highly consistent with an excitation regime situated at or well beyond the exciton Mott transition. Driven by these mechanisms, the optical properties of the material will change, leading to a measurable change in the transmission of the probe beam. However, the relative contribution and temporal evolution of these mechanisms can vary significantly between the two cases due to differences in their band structures, carrier relaxation pathways, and interlayer interactions. Earlier reports by Bera *et al* and Katsch *et al* established that elevating carrier densities beyond the Mott limit leads to a simultaneous shift and broadening of the excitonic resonances, [56, 57]. While both phenomena inherently contribute to the modulated transmission signal, linewidth broadening is conventionally the dominant factor when exciton–exciton and exciton–phonon interactions prevail. Crucially, however, Bera *et al* demonstrated that the emergence of a high-density electron–hole plasma above the Mott threshold drives bandgap renormalization, leading to reduced transmission (-ve initial peak in $\Delta T/T$ both in MoL and MuL), which is dominant in our studies, resulting in a pronounced redshift of the exciton peak. Since excitonic annihilation into an electron–hole plasma occurs rapidly at the early stages of photoexcitation, it is expected that the exciton peak shift serves as the primary mechanism governing the observed transient transmission changes, overshadowing the contribution from peak broadening.

In this study, carriers are excited at the A-exciton transition energy. At this energy, the absorption coefficient of a MoL MoS_2 is approximately 40% higher than that of MuL MoS_2 [58]. Assuming each absorbed photon generates one electron–hole pair, the carrier density in MoL is expected to be 40% higher than in MuL MoS_2. Consequently, a larger $|\Delta T/T|_{\text{peak}}$ would be anticipated for MoL. However, experimental observations reveal the opposite, with MuL exhibiting a higher $|\Delta T/T|_{\text{peak}}$ (figure 4). This contradiction can be explained by the lower exciton binding energy in MuL, which facilitates more efficient exciton dissociation compared to MoL [15, 41, 42]. The weaker binding energy of the exciton is coming from the multilayered structure of the MuL. This further leads to stronger dielectric screening and availability of additional intervalley scattering. In addition, in MuL MoS_2, the optical absorption and dielectric response seen by the probe is also modified [15, 59]. This results in a higher density of free carriers near the band edge in MuL leading to stronger BGR, despite its lower absorption. This BGR is driven by many-body Coulomb interaction, inducing a reconfiguration of the electronic band structure and reducing the bandgap energy. This accumulation of the free carriers screens the electron–hole Coulomb attraction, causing a redshift in exciton binding energy [14, 60]. Thus, the larger $|\Delta T/T|_{\text{Peak}}$ observed in MuL is attributed to its greater exciton dissociation efficiency and stronger BGR at comparable excitation densities (figure 4). Over time, the free carriers in MuL are expected to decay to defect states and also form hot carriers via Auger and defect-assisted Auger processes as that of MoL MoS_2

[32, 45–47]. The auger scattering not only contributes to the relaxation of some carriers but also excites an equal number of carriers to the higher excited states (figure 6(a)). As these carriers relax to the band edge, eventually excitons will start forming again due to lower carrier density as compared to the initial excitation condition. Such formation of the A-exciton would lead to bleaching of available states for absorption of the probe, leading to an increase in pump transmission which is stronger in MoL MoS_2 even during lower pump fluences leading to a later band bleaching with a positive peak in $\Delta T/T$. The band bleaching will give a positive contribution to the $\Delta T/T$ canceling the negative effect of BGR. Thus, the action of Auger should also be coupled with the bleaching of states later and we attribute this to the formation of excitons in the present case.

Additionally, a significant fraction of electrons relax to *Q*-valley in MuL within tens of femtoseconds, leaving holes at *K* valley [51]. These *Q*-valley electrons have lifetimes of several picoseconds [51, 52]. Although some carriers relax to defect states, a substantial population remains in the conduction band as free carriers in MuL. Moreover, since these carriers occupy different valleys, the Auger and defect-assisted Auger recombination processes are less efficient in MuL. Additionally, the greater thickness of MuL MoS_2, enhances the dielectric screening and reduces quantum confinement compared to MoL. These factors weaken the Coulombic interaction, further suppressing Auger scattering processes [56, 61]. Consequently, carrier relaxation is slower in MuL, resulting in longer recovery times for transient signals (figure 5). For instance, at a pump fluence of 2.5 mJ cm^{-2}, the decay time of MuL is $\sim$ 4.8 ps, whereas in MoL, it is $\sim$ 0.4 ps. Similarly, at a higher fluence of 7 mJ cm^{-2} pump fluence, carrier relaxation time in MuL is about 1 ps while in the case of MoL, it is 0.2 ps. Furthermore, excitation at 7.5 mJ cm^{-2} pump fluence generates a high density of hot phonons in MuL MoS_2 leading to phonon bottlenecking effect due to reabsorption of the hot phonons as that of MoL which turns the BGR to BF as shown in figure 3(a). At high excitation density, Auger-assisted relaxation and hot-carrier cooling generate a larger phonon population. These phonons are being reabsorbed by the carriers in defect states and repopulate the A-exciton state. This additional back-transfer further slows the overall decay, reinforcing the bottleneck effect, [35]. This process is an intrinsic nonequilibrium effect of the photoexcited samples under high excitation density, where a large population of carriers and emitted phonons are created within an ultrashort time window. reabsorption of hot phonons by carriers can slow carrier cooling, and the reduction in the number of available final states, including partial saturation of defect-assisted relaxation channels, can further prolong the relaxation process. However, the bottlenecking effect is more prominent in MoL and arises at significantly lower pump fluence compared to MuL. This difference is attributed to the intervalley scattering in MuL, which provides multiple relaxation pathways for carriers, unlike MoL, where excitation and relaxation of the carriers primarily occur at the *K* valley. Further, intervalley scattering and relaxation in MuL also reduce the possibility of the formation of A-excitons. Consequently, the bleaching of $\Delta T/T$ in MuL MoS_2 is much weaker and only becomes evident at much higher excitation fluence.

3. Conclusion

In this article, we have demonstrated that the ultrafast responses of MoL and MuL MoS_2 differ significantly under excitation by ultrashort pulses. These studies were carried out at high photoexcitation densities in the range of $\sim 6.6 \times 10^{13}$ cm^{-2} to $\sim 4.16 \times 10^{14}$ cm^{-2}. In spite of the fact that the MuL has a lower excitation density as compared to MoL, it still exhibited a higher change in $|\Delta T/T|_{\text{Peak}}$ when compared to that of MoL MoS_2 and clear saturation behavior, since the dissociation of excitons is much easier in MuL due to the lower exciton binding energy. Both MuL and MoL show Auger and defect-assisted Auger recombination and a positive change in $\Delta T/T$ at later times, but the MuL shows a much longer recovery time and a small positive change in $\Delta T/T$ at high excitation densities. Both of these changes are attributed to the carriers scattered to other valleys in the conduction band, which increases the carrier lifetime by suppressing exciton formation. The insights gained from these studies contribute to the understanding of ultrafast carrier dynamics in MoS_2 and are expected to aid in the development of optoelectronics applications involving MoL and MuL MoS_2, such as lasers, OPAs, and detectors.

Acknowledgments

All authors sincerely thank Mr Vijay Singh Dawer for his assistance during the measurements. The experiments presented in this work were conducted while all authors were affiliated with the Nano Science Laboratory, Materials Science section, Raja Ramanna Centre for Advanced Technology (RRCAT),

Indore. D.P.K. and S.G. acknowledge financial support from RRCAT, Indore, under the HBNI PhD program. J.J. gratefully acknowledges funding from the Deutsche Forschungsgemeinschaft (DFG, German Research Foundation) through Project No. BO1823/12 — FOR 5249 (QUAST).

Data availability statement

The data that support the findings of this study are available from the corresponding author upon reasonable request. The data cannot be made publicly available upon publication due to legal restrictions preventing unrestricted public distribution.

Supporting information available at https://doi.org/10.1088/1361-648X/ae82a8/data1.

Conflict of interest

The authors declare that they have no known competing financial interests or personal relationships that could have appeared to influence the work reported in this paper.

Author contributions

Durga Prasad Khatua 0000-0001-7712-2469
Data curation (lead), Formal analysis (lead), Investigation (lead), Methodology (lead), Resources (equal), Software (equal), Validation (lead), Visualization (lead), Writing – original draft (lead)

Asha Singh 0000-0002-8440-6256
Data curation (supporting), Formal analysis (supporting), Investigation (supporting), Validation (supporting), Visualization (supporting), Writing – review & editing (supporting)

Sabina Gurung 0000-0002-2947-8003
Formal analysis (supporting), Investigation (supporting), Validation (supporting), Visualization (supporting), Writing – review & editing (supporting)

J Jayabalan 0000-0003-4505-2712
Conceptualization (equal), Data curation (equal), Formal analysis (supporting), Funding acquisition (lead), Investigation (equal), Project administration (lead), Resources (lead), Supervision (lead), Validation (supporting), Visualization (supporting), Writing – review & editing (lead)

References

[1] Mak K F, Lee C, Hone J, Shan J and Heinz T F 2010 Atomically thin MoS_2: a new direct-gap semiconductor *Phys. Rev. Lett.* **105** 136805
[2] Splendiani A, Sun L, Zhang Y, Li T, Kim J, Chim C-Y, Galli G and Wang F 2010 Emerging photoluminescence in monolayer MoS_2 *Nano Lett.* **10** 1271
[3] Lembke D and Kis A 2012 Breakdown of high-performance monolayer MoS_2 transistors *ACS Nano* **6** 10070
[4] Zheng H, Yang B, Wang D, Han R, Du X and Yan Y 2014 Tuning magnetism of monolayer MoS_2 by doping vacancy and applying strain *Appl. Phys. Lett.* **104** 132403
[5] Luo Y K, Xu J, Zhu T, Wu G, McCormick E J, Zhan W, Neupane M R and Kawakami R K 2017 Opto-valleytronic spin injection in monolayer MoS_2/few-layer graphene hybrid spin valves *Nano Lett.* **17** 3877
[6] Kim S *et al* 2012 High-mobility and low-power thin-film transistors based on multilayer MoS_2 crystals *Nat. Commun.* **3** 1011
[7] Xie Y *et al* 2017 Ultrabroadband MoS_2 photodetector with spectral response from 445 to 2717 nm *Adv. Mater.* **29** 1605972
[8] Singh E, Kim K S, Yeom G Y and Nalwa H S 2017 Atomically thin-layered molybdenum disulfide (MoS_2) for bulk-heterojunction solar cells *ACS Appl. Mater. Interfaces* **9** 3223–45
[9] Singh E, Singh P, Kim K S, Yeom G Y and Nalwa H S 2019 Flexible molybdenum disulfide (MoS_2) atomic layers for wearable electronics and optoelectronics *ACS Appl. Mater. Interfaces* **11** 11061–105
[10] Lazanas A C and Prodromidis M I 2021 Two-dimensional inorganic nanosheets: production and utility in the development of novel electrochemical (bio) sensors and gas-sensing applications *Microchim. Acta* **188** 1–34
[11] Brumme T, Calandra M and Mauri F 2015 First-principles theory of field-effect doping in transition-metal dichalcogenides: structural properties, electronic structure, hall coefficient and electrical conductivity *Phys. Rev. B* **91** 155436
[12] Yuan L, Wang T, Zhu T, Zhou M and Huang L 2017 Exciton dynamics, transport and annihilation in atomically thin two-dimensional semiconductors *J. Phys. Chem. Lett.* **8** 3371
[13] Chernikov A, Berkelbach T C, Hill H M, Rigosi A, Li Y, Aslan O B, Reichman D R, Hybertsen M S and Heinz T F 2014 Exciton binding energy and nonhydrogenic rydberg series in monolayer WS_2 *Phys. Rev. Lett.* **113** 076802
[14] Ugeda M M *et al* 2014 Giant bandgap renormalization and excitonic effects in a monolayer transition metal dichalcogenide semiconductor *Nat. Mater.* **13** 1091

[15] Borzda T *et al* 2015 Charge photogeneration in few-layer MoS_2 *Adv. Funct. Mater.* **25** 3351
[16] Evans B and Young P 1967 Exciton spectra in thin crystals: the diamagnetic effect *Proc. Phys. Soc.* **91** 475
[17] Lee K J, Xin W and Guo C 2020 Annihilation mechanism of excitons in a MoS_2 monolayer through direct förster-type energy transfer and multistep diffusion *Phys. Rev. B* **101** 195407
[18] Tsai H-S, Huang Y-H, Tsai P-C, Chen Y-J, Ahn H, Lin S-Y and Lu Y-J 2020 Ultrafast exciton dynamics in scalable monolayer MoS_2 synthesized by metal sulfurization *ACS Omega* **5** 10725
[19] Srivastava Y K, Chaturvedi A, Manjappa M, Kumar A, Dayal G, Kloc C and Singh R 2017 MoS_2 for ultrafast all-optical switching and modulation of thz fano metaphotonic devices *Adv. Opt. Mater.* **5** 1700762
[20] Zhang T and Wang J 2021 Defect-enhanced exciton–exciton annihilation in monolayer transition metal dichalcogenides at high exciton densities *ACS Photonics* **8** 2770–80
[21] Chi Z, Chen H, Zhao Q and Weng Y-X 2020 Observation of the hot-phonon effect in monolayer MoS_2 *Nanotechnology* **31** 235712
[22] Wang W, Sui N, Chi X, Kang Z, Zhou Q, Li L, Zhang H, Gao J and Wang Y 2021 Investigation of hot carrier cooling dynamics in monolayer MoS_2 *J. Phys. Chem. Lett.* **12** 861
[23] Pan C, Jiang L, Sun J, Wang Q, Wang F, Wang K, Lu Y, Wang Y, Qu L and Cui T 2020 Ultrafast optical response and ablation mechanisms of molybdenum disulfide under intense femtosecond laser irradiation *Light Sci. Appl.* **9** 1
[24] Völzer T, Fennel F, Korn T and Lochbrunner S 2021 Fluence-dependent dynamics of localized excited species in monolayer versus bulk MoS_2 *Phys. Rev. B* **103** 045423
[25] Águila A G D *et al* 2023 Ultrafast exciton fluid flow in an atomically thin MoS_2 semiconductor *Nat. Nanotechnol.* **18** 1012–9
[26] Girotto N, Caruso F and Novko D 2023 Ultrafast nonadiabatic phonon renormalization in photoexcited single-layer MoS_2 *J. Phys. Chem. C* **127** 16515–24
[27] Xu C *et al* 2023 Ultrafast electronic relaxation dynamics of atomically thin MoS_2 is accelerated by wrinkling *ACS Nano* **17** 16682–94
[28] Trovatello C *et al* 2021 Optical parametric amplification by monolayer transition metal dichalcogenides *Nat. Photon.* **15** 6–10
[29] Zhao G, Hou J, Wu Y, He J and Hao X 2015 Preparation of 2D MoS_2/graphene heterostructure through a monolayer intercalation method and its application as an optical modulator in pulsed laser generation *Adv. Opt. Mater.* **3** 937
[30] Zhou Y H, An H N, Gao C, Zheng Z Q and Wang B 2019 Uv–vis-nir photodetector based on monolayer MoS_2 *Mater. Lett.* **237** 298
[31] Liu F, Ziffer M E, Hansen K R, Wang J and Zhu X 2019 Direct determination of band-gap renormalization in the photoexcited monolayer MoS_2 *Phys. Rev. Lett.* **122** 246803
[32] Wang H, Zhang C and Rana F 2015 Surface recombination limited lifetimes of photoexcited carriers in few-layer transition metal dichalcogenide MoS_2 *Nano Lett.* **15** 8204
[33] DLayer 2020 2dlayer (available at: https://2dlayer.com procured from 2 Davis Drive)
[34] Zhang C, Wang H, Chan W, Manolatou C and Rana F 2014 Absorption of light by excitons and trions in monolayers of metal dichalcogenide MoS_2: Experiments and theory *Phys. Rev. B* **89** 205436
[35] Khatua D P, Singh A, Gurung S and Jayabalan J 2022 Excitation density dependent carrier dynamics in a monolayer MoS_2: Exciton dissociation, formation and bottle necking *Micro Nanostruct.* **165** 207205
[36] Khatua D P, Singh A, Gurung S, Tanwar M, Kumar R and Jayabalan J 2022 A comparative study of ultrafast carrier dynamics near A, B and C-excitons in a monolayer MoS_2 at high excitation densities *Opt. Mater.* **126** 112224
[37] Khatua D P, Singh A, Gurung S, Khan S and Jayabalan J 2022 Ultrafast carrier dynamics in a monolayer MoS_2 at carrier densities well above mott density *J. Phys.: Condens. Matter* **34** 155401
[38] Song B, Gu H, Fang M, Chen X, Jiang H, Wang R, Zhai T, Ho Y-T and Liu S 2019 Layer-dependent dielectric function of wafer-scale 2d MoS_2 *Adv. Opt. Mater.* **7** 1801250
[39] Yu K, Wang J, Chen J and Wang G P 2019 Inhomogeneous photocarrier dynamics and transport in monolayer MoS_2 by ultrafast microscopy *Nanotechnology* **30** 485701
[40] Ceballos F, Cui Q, Bellus M Z and Zhao H 2016 Exciton formation in monolayer transition metal dichalcogenides *Nanoscale* **8** 11681
[41] Nie Z, Long R, Sun L, Huang C-C, Zhang J, Xiong Q, Hewak D W, Shen Z, Prezhdo O V and Loh Z-H 2014 Ultrafast carrier thermalization and cooling dynamics in few-layer MoS_2 *ACS Nano* **8** 10931
[42] Nie Z, Long R, Teguh J S, Huang C-C, Hewak D W, Yeow E K, Shen Z, Prezhdo O V and Loh Z-H 2015 Ultrafast electron and hole relaxation pathways in few-layer MoS_2 *J. Phys. Chem. C* **119** 20698
[43] Wang L *et al* 2017 Slow cooling and efficient extraction of C-exciton hot carriers in MoS_2 monolayer *Nat. Commun.* **8** 1
[44] Sun D, Rao Y, Reider G A, Chen G, You Y, Brézin L, Harutyunyan A R and Heinz T F 2014 Observation of rapid exciton–exciton annihilation in monolayer molybdenum disulfide *Nano Lett.* **14** 5625
[45] Cha S, Sung J H, Sim S, Park J, Heo H, Jo M-H and Choi H 2016 1 s-intraexcitonic dynamics in monolayer MoS_2 probed by ultrafast mid-infrared spectroscopy *Nat. Commun.* **7** 1
[46] Schiettecatte P, Geiregat P and Hens Z 2019 Ultrafast carrier dynamics in few-layer colloidal molybdenum disulfide probed by broadband transient absorption spectroscopy *J. Phys. Chem. C* **123** 10571–7
[47] Seo M, Yamaguchi H, Mohite A D, Boubanga-Tombet S, Blancon J-C, Najmaei S, Ajayan P M, Lou J, Taylor A J and Prasankumar R P 2016 Ultrafast optical microscopy of single monolayer molybdenum disulfide flakes *Sci. Rep.* **6** 1
[48] Berkelbach T C, Hybertsen M S and Reichman D R 2013 Theory of neutral and charged excitons in monolayer transition metal dichalcogenides *Phys. Rev. B* **88** 045318
[49] Wang H, Zhang C and Rana F 2015 Ultrafast dynamics of defect-assisted electron–hole recombination in monolayer MoS_2 *Nano Lett.* **15** 339
[50] He X, Chebl M and Yang D-S 2020 Cross-examination of ultrafast structural, interfacial and carrier dynamics of supported monolayer MoS_2 *Nano Lett.* **20** 2026
[51] Wallauer R, Reimann J, Armbrust N, Güdde J and Höfer U 2016 Intervalley scattering in MoS_2 imaged by two-photon photoemission with a high-harmonic probe *Appl. Phys. Lett.* **109** 162102
[52] Kumar N, He J, He D, Wang Y and Zhao H 2013 Charge carrier dynamics in bulk MoS_2 crystal studied by transient absorption microscopy *J. Appl. Phys.* **113** 133702
[53] Chernikov A, Ruppert C, Hill H M, Rigosi A F and Heinz T F 2015 Population inversion and giant bandgap renormalization in atomically thin WS_2 layers *Nat. Photon.* **9** 466
[54] Pogna E A *et al* 2016 Photo-induced bandgap renormalization governs the ultrafast response of single-layer MoS_2 *ACS Nano* **10** 1182–8

[55] Sim S, Park J, Song J-G, In C, Lee Y-S, Kim H and Choi H 2013 Exciton dynamics in atomically thin MoS_2: interexcitonic interaction and broadening kinetics *Phys. Rev. B* **88** 075434
[56] Bera S K, Shrivastava M, Bramhachari K, Zhang H, Poonia A K, Mandal D, Miller E M, Beard M C, Agarwal A and Adarsh K 2021 Atom like interaction and optically tunable giant band-gap renormalization in large-area atomically thin MoS_2 *Phys. Rev. B* **104** L201404
[57] Katsch F, Selig M and Knorr A 2020 Exciton-scattering-induced dephasing in two-dimensional semiconductors *Phys. Rev. Lett.* **124** 257402
[58] Castellanos-Gomez A, Quereda J, van der Meulen H P, Agraït N and Rubio-Bollinger G 2016 Spatially resolved optical absorption spectroscopy of single-and few-layer MoS_2 by hyperspectral imaging *Nanotechnology* **27** 115705
[59] Ermolaev G A *et al* 2020 Broadband optical properties of monolayer and bulk MoS_2 *npj 2D Mater. Appl.* **4** 21
[60] Cunningham P D, Hanbicki A T, McCreary K M and Jonker B T 2017 Photoinduced bandgap renormalization and exciton binding energy reduction in WS_2 *ACS Nano* **11** 12601–8
[61] Sim S, Shin H-S, Lee D, Lee J, Cha M, Lee K and Choi H 2021 Opposite behavior of ultrafast dynamics of exciton shift and linewidth broadening in bilayer ReS_2 *Phys. Rev. B* **103** 014309